

Accepted Manuscript

Title: Efficient conversion of furfural into cyclopentanone over high performing and stable Cu/ZrO₂ catalysts

Authors: Yifeng Zhang, Guoli Fan, Lan Yang, Feng Li

PII: S0926-860X(18)30260-6
DOI: <https://doi.org/10.1016/j.apcata.2018.05.030>
Reference: APCATA 16679

To appear in: *Applied Catalysis A: General*

Received date: 15-3-2018
Revised date: 8-5-2018
Accepted date: 25-5-2018

Please cite this article as: Zhang Y, Fan G, Yang L, Li F, Efficient conversion of furfural into cyclopentanone over high performing and stable Cu/ZrO₂ catalysts, *Applied Catalysis A, General* (2018), <https://doi.org/10.1016/j.apcata.2018.05.030>

This is a PDF file of an unedited manuscript that has been accepted for publication. As a service to our customers we are providing this early version of the manuscript. The manuscript will undergo copyediting, typesetting, and review of the resulting proof before it is published in its final form. Please note that during the production process errors may be discovered which could affect the content, and all legal disclaimers that apply to the journal pertain.



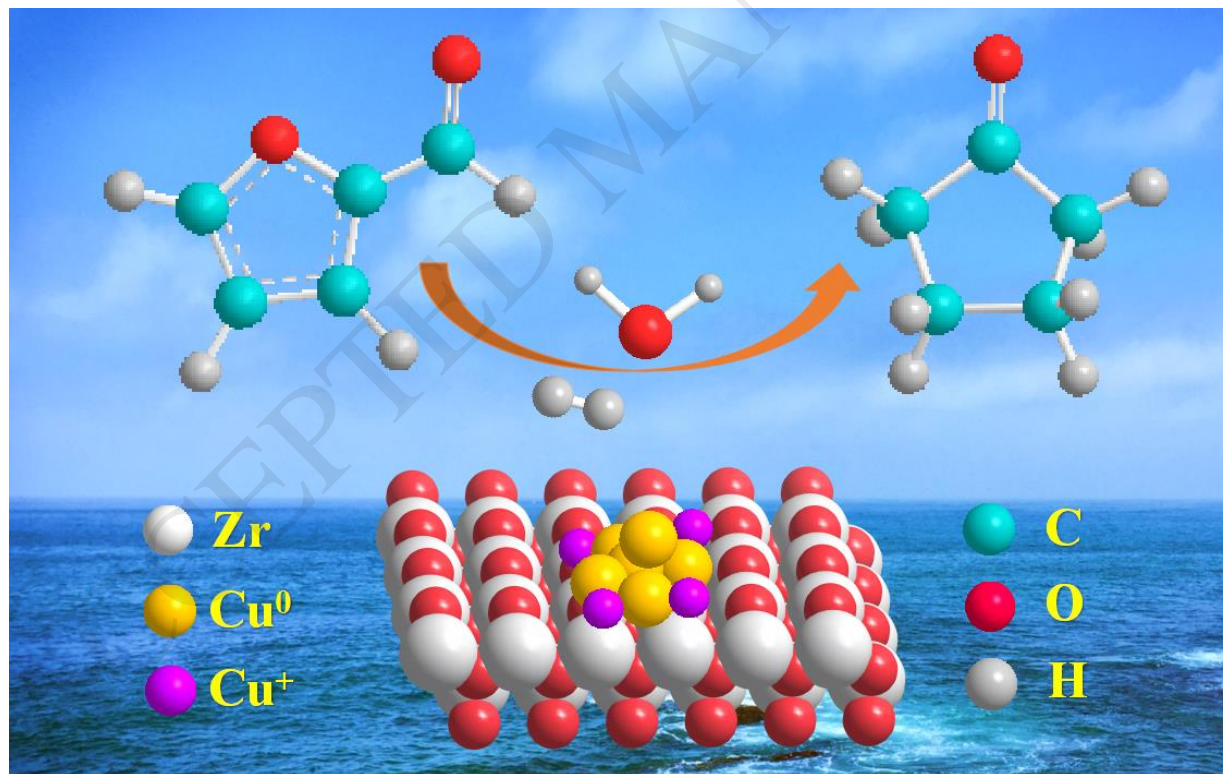
Efficient conversion of furfural into cyclopentanone over high performing and stable Cu/ZrO₂ catalysts

Yifeng Zhang, Guoli Fan, Lan Yang, Feng Li*

State Key Laboratory of Chemical Resource Engineering, Beijing Advanced Innovation Center for Soft Matter Science and Engineering, Beijing University of Chemical Technology, Beijing, 100029, China.

* Tel.: +8610-64451226; fax: +8610-64425385. E-mail: lifeng@mail.buct.edu.cn

Graphical abstract



Highlights

- High performing and stable supported Cu-based catalysts were facilely fabricated.
- Strong interactions between Cu species and the ZrO₂ support were formed.
- Highly efficient conversion of furfural into cyclopentanone was achieved.
- Surface Cu⁺-acidic site synergistic effect on the CPO formation was confirmed.

ABSTRACT: Currently, biomass transformation to produce high value-added chemicals and liquid biofuels is attracting more and more interest by the virtue of its importance in the sustainable development of human society. Herein, we reported the conversion of furfural (FFA) into cyclopentanone (CPO) in water over high performing and stable Cu/ZrO₂ catalysts prepared by our developed one-pot reduction-oxidation method. It was demonstrated that surface structures and catalytic performances of catalysts could be delicately adjusted by varying the calcination temperatures for catalyst precursors. Especially, an appropriate calcination temperature of 500 °C could significantly enhance the interactions between surface Cu species and the ZrO₂ support, thus greatly facilitating the formation of Cu⁺-O-Zr-like structure at the metal-support interface, and the resulting Cu/ZrO₂ catalyst showed a superior catalytic performance with a high CPO yield of 91.3 % under mild reaction conditions (*i.e.* a low hydrogen pressure of 1.5 MPa and 150 °C) to other metal oxides supported copper catalysts prepared by the conventional impregnation. It was revealed that in addition to surface acidic sites, surface Cu⁺/(Cu⁰+Cu⁺) ratio also played a key role in promoting the formation of CPO in the present Cu/ZrO₂ catalytic system.

KEYWORDS: *Copper; Zirconia; Metal-support interactions; Surface structure; Hydrogenation.*

1. Introduction

With the decrease of global fossil resources, energy crisis caused by the increasing consumption of fossil fuels (coal and oil) and the resulting environmental pollution are becoming more and more serious all over the world. As a kind of renewable and sustainable resource and the best alternative to fossil fuels, biomass has attracted broad research attention, because its efficient transformation into important chemicals and high value-added liquid biofuels can not only decline the dependence on fossils but also reduce environmental pollution [1-3]. For example, furfural (FFA), a most important and significant biomass-derived platform compound from hemicellulose and xylose [4-9], can be converted through hydrogenation/hydrogenolysis processes to produce various chemicals, nonpetroleum-derived liquid fuels, and fuel additives (*e.g.* furfuryl alcohol (FAL), tetrahydrofurfuryl alcohol (THFA), 2-methylfuran, tetrahydrofuran, γ -valerolactone, and pentadiol) [10-17].

Cyclopentanone (CPO), as an important intermediate, is used to manufacture a wide range of chemicals (*e.g.* medicines, herbicides, pesticides, and perfumes) [18], fuel precursors and high-density fuels through condensation-hydrogenation process [19,20]. In industry, CPO is mainly produced by the pyrolysis of adipic acid and its derivatives or the direct oxidation of cyclopentene [21-23]. However, the former simultaneously produces large numbers of pollutants, while the latter always affords low CPO yields under harsh reaction conditions including high reaction temperatures and/or high pressures. Fortunately, it was recently reported that CPO could be obtained by the hydrogenation of biomass-derived FFA in neat water over various supported noble metal catalysts [24-28], especially, along with a high yield of 92.1% over the Pd-Cu/C catalyst under a hydrogen pressure of 3.0 MPa at 160 °C [26], and even a quantitative conversion of FFA into CPO over the Au/TiO₂ under a hydrogen pressure of 4.0 MPa [27]. As for bimetallic Pd-Cu/C catalyst, it was shown that the synergy between Pd⁰-Cu⁺ species contributed to a good catalytic activity [26]. Very recently, Ru-based catalyst has been reported to efficiently catalyze the FFA hydrogenation to generate CPO under a hydrogen pressure of 1.0 MPa [28]. Taking into consideration high costs of precious metals, non-precious copper, nickel and bimetallic Cu-Ni catalysts also were developed for the above reaction [29-34]. For non-precious metal catalysts,

however, relatively high reaction temperatures and/or hydrogen pressures adopted greatly limit their large-scale industrial application. Therefore, developing high performing non-precious metal catalytic systems for the synthesis of CPO has important implications for practical applications.

To achieve the high CPO selectivity in the FFA hydrogenation, it is necessary for catalytically active sites on catalysts to be able to significantly promote the rearrangement of formed FAL intermediate to obtain CPO. It was reported that interfacial Cu^+ species formed in the case of Cu-based catalysts could function as active sites activating the C=O bond in FFA to some extent [29,35], while surface Lewis acidic sites favored the FAL rearrangement [36]. On the other side, it is well known that the metal-support interactions can greatly affect the catalytic performance of catalysts. For example, the strong interactions between copper species and metal oxides could improve the catalytic performances in large numbers of hydrogenation reactions [37-40]. Recently, we also reported that supported Cu catalysts showed good catalytic performances in the transformation of γ -valerolactone to valerate esters with the help of surface Cu^+ species [41,42].

In this contribution, we synthesized a series of Cu/ZrO₂ catalysts by our developed one-pot reduction-oxidation route for the transformation of FFA to produce CPO, and especially investigated the effect of the calcination temperature for catalyst precursors on the surface structures and catalytic performances of the resulting copper-based catalysts to unravel the role of metal-support interactions in affecting the catalytic performance. It was shown that as-formed Cu/ZrO₂ catalyst at a calcination temperature of 500 °C exhibited an excellent catalytic performance under mild reaction conditions (*e.g.* a quite low hydrogen pressure of 1.5 MPa and 150 °C), along with a quite high CPO yield of 91.3 %, indicative of the superiority to other metal oxides supported copper catalysts prepared by the conventional impregnation. High catalytic efficiency of the catalyst mainly resulted from the occurrence of strong metal-support interactions (SMSIs) facilitating the formation of surface Cu^+ species, as well as favorable

surface acidity. To the best of our knowledge, there is no report about using such high performing and stable Cu/ZrO₂ catalyst for the conversion of FFA to produce CPO up to now.

2. Experimental section

2.1 Preparation of Cu/ZrO₂ catalysts

A series of Cu/ZrO₂ catalysts were prepared by our developed one-pot reduction-oxidation method [41]. Firstly, Zr(NO₃)₄·5H₂O (0.01mol, 4.293g) and Cu(NO₃)₂·3H₂O (0.01mol, 2.416g) were dissolved into 80 ml of deionized water to form a salt solution A, while NaBH₄ (0.2 mol, 7.59g) was dissolved into 80 ml of deionized water to obtain a solution B. Subsequently, above two solutions were simultaneously added to a colloid mill, and at once mixed rapidly at a rotor speed of 3000 rpm for 3 min. Afterwards, the resulting suspension was transferred to a Teflon-lined autoclave reactor and aged at 150 °C for 48 h. The obtained precipitate was washed with deionized water until pH = 7.0 and dried at 70 °C overnight. Then, the obtained solid (denoted as CuO/ZrO₂-R) was calcined at different temperatures of 400, 500 or 600 °C under air atmosphere and held for 6 h to obtain calcined CuO/ZrO₂-*x* catalyst precursors (*x* represents the calcination temperature). At last, CuO/ZrO₂ samples were reduced in 10% v/v H₂/Ar atmosphere at 300 °C for 2h to gain Cu/ZrO₂-R and Cu/ZrO₂-*x* catalysts. In addition, pure ZrO₂-500 support also was synthesized according to the similar procedure to that for CuO/ZrO₂-500 without the addition of Cu(NO₃)₂·3H₂O. For comparison, different metal oxides supported Cu catalysts with the similar copper loadings (*i.e.* Cu/ZrO₂-im, Cu/MgO-im, Cu/ZnO-im and Cu/Al₂O₃-im) were synthesized by the conventional impregnation method.

2.2 Characterization

Shimadzu XRD-6000 diffractometer with a graphite-filtered Cu K_α source ($\lambda = 0.15418$ nm) at 40 kV and 30 mA was utilized to obtain X-ray diffraction (XRD) patterns of samples.

Elemental analysis was carried out using a Shimadzu ICPS-7500 inductively coupled plasma atomic emission spectroscopy (ICP-AES).

Transmission electron microscopy (TEM) images were obtained on a JEOL JEM-2100 electron microscope. N₂ adsorption-desorption experiments of samples were performed on a Micromeritics ASAP 2020 sorptometer apparatus.

Hydrogen temperature-programmed reduction (H₂-TPR) and ammonia temperature-programmed desorption (NH₃-TPD) experiments were carried out on a Thermo Fisher TPDRO-1100 chemical adsorption instrument with a thermal conductivity detector (TCD). For H₂-TPR, the sample (100 mg) was degassed under Ar flow at 200 °C for 2h. Afterwards, TPR measurement was executed in a flow of 10% H₂/Ar (30 mL min⁻¹) with a heating rate of 10 °C min⁻¹ from 50 to 800 °C. For NH₃-TPD, the sample (100 mg) was reduced in a flow of 10% H₂/Ar atmosphere at 300 °C for 2h with a ramping rate of 5 °C min⁻¹, and then cooled to room temperature. Subsequently, the sample was degassed at 300 °C for 1h under He flow and followed by treatment with a 5% NH₃/He flow for 1.5 h at 100 °C. Then, chemisorbed NH₃ was desorbed by heating at a ramping rate of 10 °C min⁻¹ up to 900 °C.

X-ray photoelectron spectra (XPS) was recorded on a Thermo VG ESCALAB250 X-ray photoelectron spectrometer using a monochromatic Al K_α radiation of 1486.6 eV photons. The graphite C_{1s} peak at 284.6 eV was used to calibrate all binding energies.

Active copper surface areas of samples were determined by N₂O titration using a Micromeritics ChemiSorb 2920 instrument. Firstly, a H₂-TPR process under a 10% H₂/Ar flow (40mL min⁻¹) from 50 to 300 °C was conducted on the calcined sample (100 mg). Secondly, after the reduced sample was oxidized with a flow of 10% N₂O/N₂ (40mL min⁻¹) at 70 °C for 1h, residual N₂O was removed under an Ar flow. Finally, H₂-TPR was carried out again from room temperature to 300 °C. Cu surface area was obtained based on spherical shape of metal particles and surface concentration of 1.47×10^{19} Cu atoms on per m².

In situ infrared spectra (IR) of pyridine (Py) adsorption was collected on a Thermo Nicolet 380 FT-IR spectrometer. First, the self-supporting wafer of reduced sample (30 mg), which was placed into an evacuable IR cell with CaF₂ windows, was evacuated at 200 °C for 1h under argon

flow. Then, pyridine was introduced and held for 1h. Finally, IR spectra were recorded after physisorbed pyridine was removed by evacuation.

2.3 Catalytic FFA hydrogenation tests

Typically, FFA (5 mmol, 0.48 g), catalyst (0.05 g) and ultrapure water (15 ml) were placed into a stainless-steel autoclave reactor with a magnetic stirrer, and then the reactor was sealed and flushed with pure hydrogen for ten times. Subsequently, the reactor was charged with pure hydrogen under atmospheric pressure. After that, the reactor was heated to certain reaction temperature (typically 150 °C) at a heating rate of 10 °C/min and then hydrogen was further fed into the reactor up to certain reaction pressure (typically 1.5 MPa). The reaction was initiated by stirring at a speed of 1000 rpm. During the reaction, the hydrogen pressure was kept constant by supplying hydrogen continuously from gas cylinder through the pressure regulator to compensate for the consumed hydrogen in the reactor. After the reaction, the reactor was rapidly cooled to room temperature and then depressurized. The organic products were extracted by dichloromethane from the liquid and then analyzed by gas chromatograph (Agilent 7890B) equipped with a DB-WAX capillary column (30.0 m × 250 μm × 0.25 μm) and identified as compared with known standards using dodecane as an internal standard. The used catalyst was recycled from the reaction solution by centrifugation and washed several times with deionized water and ethanol before the next cyclic test.

3. Results and discussion

3.1 Structural characterization

Fig.1A presents the XRD patterns of different CuO/ZrO₂ catalyst precursors. In each case, four diffractions appearing at 2θ of about 30.2°, 35.2°, 50.4° and 60.2° are indexed as the (011), (110), (020) and (121) planes of tetragonal ZrO₂ (*t*-ZrO₂) phase (JCPDS 50-1089), respectively. As the calcination temperature is elevated, no obvious change in diffractions assignable to *t*-ZrO₂ is found, indicative of the formation of stable *t*-ZrO₂ phase in all precursors. Interestingly, for

CuO/ZrO₂-R sample, one can see another diffraction at about 43.2°, which is assigned to the (111) plane of metallic Cu phase (JCPDS 04-0836). In the XRD patterns of CuO/ZrO₂ samples, no diffractions related to metallic Cu can be observed; While a new diffraction corresponding to the (111) plane of CuO phase (JCPDS 05-667) appear at about 38.5° due to the oxidation of metallic Cu and is enhanced gradually with the elevated calcination temperature. As shown in Fig.1B, for reduced Cu/ZrO₂ samples, in addition to those for *t*-ZrO₂ phase, the intensive (111) diffraction for metallic Cu phase can be observed, owing to the complete reduction of CuO phase in precursors. The average size of Cu⁰ particles was calculated based on Scherrer equation (Table 1). The Cu particle size in the Cu/ZrO₂-R is the smallest (20.2 nm), whereas that in the Cu/ZrO₂-600 is largest (30.9 nm).

Further, the microstructure of reduced Cu/ZrO₂ samples were clearly presented by TEM observations. TEM images (Fig.2) depict that large quantities of small-sized black Cu NPs are dispersed on the surface and with the elevated calcination temperature, more serious agglomeration of NPs can be observed. Obviously, the average Cu particle sizes in Cu/ZrO₂ samples estimated by TEM are much smaller than those based on the XRD results (Table 1). In general, the smaller the particles, the lower the order of the atoms, the more difficult it is to be detected by XRD. Even if the samples contain only a small number of large-sized particles, the intense diffraction originating from large particles may overshadow that of small-sized particles in the XRD patterns [43]. As further evidenced by TEM images (Fig.S1), a few large-sized Cu particles can be detected in Cu/ZrO₂ samples. As it is known, smaller metal particles commonly exhibit higher hydrogenation activities compared with larger ones owing to the larger active metal surface areas and low activation energies for dissociation of hydrogen [44]. For example, it was reported that the smaller copper particles in Cu-based catalyst showed higher catalytic activities in the hydrogenation of dimethyl oxalate to methyl glycolate [45]. Therefore, we consider that in our case, a large amount of small-sized Cu particles should be more important in terms of catalytic activity, compared with a few large-sized Cu particles.

In addition, all Cu/ZrO₂ samples show type-IV N₂ adsorption-desorption isotherms, reflecting the presence of mesoporous structure (Fig.S2) [46]. The pore diameter distributions reveal that the average pore diameter of samples is slightly increased with the elevated calcination temperature, indicative of the occurrence of particle agglomeration to some extent. As summarized in Table 1, the BET specific surface area of reduced Cu/ZrO₂ samples decreases gradually with the elevated calcination temperature, due to the enhanced crystallization of *t*-ZrO₂ phase in samples, as well as more serious agglomeration of particles at higher calcination temperatures. Meanwhile, it is noted that metallic copper surface area for Cu/ZrO₂-R determined based on N₂O titration is higher (23.6 m²/g) than those for other Cu/ZrO₂ samples, in good accordance with the above XRD results.

3.2 Redox behaviors and surface electronic states of samples

The redox behaviors of CuO/ZrO₂ precursors were investigated by H₂-TPR analysis. As displayed in Fig.3, CuO/ZrO₂-R sample presents a broad peak in the temperature range of 125-210 °C, which is associated with the reduction of surface highly dispersed Cu²⁺ species. With the elevated calcination temperature to 400 °C, in addition to a relatively small peak for surface Cu²⁺ species, another large reduction peak appears at about 215 °C, mirroring the presence of a large amount of bulk CuO. In the case of CuO/ZrO₂-500, two reduction peaks for surface highly dispersed Cu²⁺ species and bulk CuO obviously shift to higher temperatures of 180 °C and 235 °C, respectively. The reduced reducibility of Cu²⁺ species for CuO/ZrO₂-500 strongly reflects the enhanced interactions between Cu²⁺ species and the ZrO₂ support, probably due to the formation of the Cu-O-Zr-like structure at the metal-support interface [41,42]. As the calcination temperature is further elevated to 600 °C, the reduction peak area for highly dispersed Cu²⁺ species is significantly decreased, despite a slight increase in the reduction temperature, mainly owing to the sintering and accumulation of surface Cu²⁺ species and thus the formation of large-sized bulk CuO in the sample. The above results demonstrate that an appropriate calcination

temperature of 500 °C is good for the enhanced interactions between Cu^{2+} species and the ZrO_2 matrix.

To determine surface electronic states of copper species on Cu/ZrO_2 samples, XPS data were obtained (Fig.4A). Clearly, in each case, $\text{Cu } 2p_{3/2}$ and $\text{Cu } 2p_{1/2}$ signals appear at about 932.6 eV and 952.5 eV, respectively, and no satellite peaks are found in the binding energy range of 940-945 eV. This means that Cu^{2+} species should be reduced to Cu^0 species and/or Cu^+ species [47]. To further discriminate between Cu^+ and Cu^0 species, the Cu LMM XAES of samples was recorded (Fig.4B). Deconvolution of the spectra clearly reveals the coexistence of Cu^0 and Cu^+ species in all samples, based on two different kinetic energy values (about 916.2 eV for Cu^+ and 918.6 eV for Cu^0 , respectively) [48,49]. Noticeably, surface $\text{Cu}^+ / (\text{Cu}^0 + \text{Cu}^+)$ ratio calculated by XAES subpeak fitting increases gradually with the calcination temperature up to 500 °C, due to the formation of more $\text{Cu}^+ \text{-O-Zr}$ -like structure at the metal-support interface thereby significantly stabilizing Cu^+ species [41]. However, the relative proportion of surface Cu^+ species in the $\text{Cu/ZrO}_2\text{-600}$ inversely decreases, which is attributable to the weakened metal-support interactions originating from the presence of a large amount of large-sized bulk CuO species in the $\text{CuO/ZrO}_2\text{-600}$ precursor.

Previous studies have demonstrated that surface acid-base properties of catalysts could greatly affect the FFA hydrogenation to form CPO [27,36]. Especially, surface weak acidic sites were beneficial to the improvement in the CPO selectivity, whereas strong acidic or basic sites was not conducive to the formation of CPO. To determine surface acidity of Cu/ZrO_2 samples, *in situ* IR spectra of adsorbed pyridine was recorded (Fig.5A). In each case, several absorption bands appearing at 1400-1700 cm^{-1} are correlated with pyridine adsorption on Lewis acidic sites (LA: 1450 cm^{-1} , 1612 cm^{-1}) and Brønsted/Lewis acidic sites (LA+BA: 1498 cm^{-1}), as well as on H-bonding adsorbed pyridine (HB: 1595 cm^{-1} , 1601 cm^{-1}) [50]. Notably, with the elevated calcination temperature, the intensities of all the absorption bands are reduced progressively and almost completely disappear in the case of $\text{Cu/ZrO}_2\text{-600}$, indicative of the reduced surface acidity. Further, surface acidity of samples was analyzed by $\text{NH}_3\text{-TPD}$ (Fig.5B). In each case, there is a

broad desorption peak in the range of 100-550 °C. Fine deconvolution of the broad peak depicts that two desorption subpeaks in the range of 100-350 °C are assigned to NH₃ desorption on weak acidic sites, while another peak to NH₃ desorption on medium-strength acidic sites [51,52]. For pristine ZrO₂-500 sample, besides three desorption subpeaks below 500 °C, two small desorption subpeaks above 500 °C are associated with strong Lewis acidic sites, confirming that Cu⁺ species should exist in the form of Cu⁺-O-Zr structure at Cu⁰-ZrO₂ interface, thus suppressing the formation of strong acidic sites. In addition, the quantitative result (Table 1) reveals that the amount of total acidic sites decreases with the calcination temperature. Interestingly, the amount of weak acidic sites on Cu/ZrO₂-400 and Cu/ZrO₂-500 samples is almost equal, probably because surface Cu⁺ species may function as Lewis acidic sites. Moreover, NH₃-TPD of pure Cu powder prepared by the one-pot reduction-oxidation method in the absence of Zr(NO₃)₄·5H₂O was performed (Fig.S3). According to the metallic surface area-normalized basis, the amount of NH₃ adsorbed on the copper powder with the copper surface area of 85 m²/g is about 0.35 μmol/m². Considering the actual metallic copper surface area of 18.5 m²/g, a tiny amount of NH₃ (0.0065 mmol/g) can be adsorbed on metallic copper sites in the case of Cu/ZrO₂-500. It further confirms that surface acidic sites on Cu/ZrO₂ samples mainly come from the ZrO₂ support and the metal-support interface.

3.3 Catalytic FFA hydrogenation

The FFA hydrogenation to produce CPO in aqueous solution is a quite complicated process (Fig.S4) [25,26], which usually can be divided into two types of reaction processes: hydrogenation and rearrangement. Firstly, the C=O bond in FFA can be selectively hydrogenated to form FAL intermediate. Secondly, FAL further rearranges in aqueous solution. Commonly, 4-hydroxycyclopentenone can be first produced through the FAL rearrangement, but it is extremely unstable in the reaction system and quickly converts to 2-cyclopentenone (2-CPEO). Thirdly, 2-CPEO is further hydrogenated to generate CPO. At last, CPL is produced by the deep hydrogenation of CPO. Meanwhile, THFA can be generated through the reduction of C=C bond

in FAL, besides small amounts of oligomers produced by the reaction between FFA and FAL. As a result, to achieve a high CPO selectivity, surface active sites on catalysts should enable the promotion of the FAL rearrangement and prevent the C=C bond hydrogenation or polymerization reactions.

The change of FFA conversion and product selectivities over different Cu/ZrO₂ catalysts with the reaction time is presented in Fig.6. It is worthwhile to note that over Cu/ZrO₂-R and Cu/ZrO₂-400, a complete conversion of FFA is achieved within 30 min, indicative of their extremely high catalytic activity. In the cases of Cu/ZrO₂-500 and Cu/ZrO₂-600, however, the complete conversion of FFA needs a longer reaction time of 2 h. During FFA hydrogenation, surface Cu⁰ sites are mainly responsible for dissociation of H₂ [35]. Meanwhile, surface Cu⁺ species were reported to enable the adsorption and activation of the C=O bond in carbonyl compounds [29,35,36], probably preventing the formation of THFA through the hydrogenation of furan ring in FFA molecule in our case. Recently, Hronec et al. also reported that Cu⁺ species played an important role in gaining excellent catalytic activity in the FFA hydrogenation into CPO because of the interaction between Cu⁺ species and the C=O bond in FFA [26]. It suggests that metallic copper species are not the sole important catalytically active sites in the FFA hydrogenation, and Cu⁺ site can function as another active site. Therefore, the higher hydrogenation activities of Cu/ZrO₂-R and Cu/ZrO₂-400 catalysts should be attributed to surface synergy between Cu⁰ and Cu⁺ species, especially the presence of more highly dispersed Cu⁰ species (Table 1). Correspondingly, in the case of Cu/ZrO₂-600, a reduced hydrogenation activity may be associated with both the smaller copper surface area and the smaller amount of surface Cu⁺ species. As shown in Table 2, despite the high activity, a lower CPO selectivity of 45.7 %, as well as higher FAL and CPL selectivities (37.7 % and 15.9 %, respectively), is obtained over the Cu/ZrO₂-R after a reaction time of 4 h, in comparison with other catalysts. It suggests that during multi-step FFA hydrogenation processes, surface Cu⁰ species are beneficial to the hydrogenation of the C=O bond in substrates (*i.e.* FFA and CPO intermediate). For Cu/ZrO₂-400 and Cu/ZrO₂-500 catalysts, initially formed FAL intermediate can rapidly convert into CPO in the initial period

of 2 h. Among these tested catalysts, Cu/ZrO₂-500 catalyst affords a highest CPO selectivity of 91.3% and a lowest FAL selectivity of 1.4 % after 4 h. It illustrates that the FAL rearrangement can proceed rapidly once FAL is formed. However, with the further increase in the reaction time from 4 h to 8 h, the CPO selectivity declines gradually, which mainly results from the deep hydrogenation of CPO and thus the formation of CPL. Compared with those over Cu/ZrO₂-400 and Cu/ZrO₂-500 catalysts, the conversion rate of FFA over the Cu/ZrO₂-600 is slower, thus leading to a decreased CPO selectivity after 4 h. Interestingly, for Cu/ZrO₂-600, the CPO selectivity almost keeps unchanged with the reaction time from 4h to 8h, due to the equal rates between FAL conversion and CPL formation at this time originating from the lower hydrogenation activity of Cu/ZrO₂-600 catalyst.

To identify the intrinsic catalytic performance of different Cu/ZrO₂ catalysts, the turnover frequency (TOF) value of FFA conversion was determined according to the rate of FFA consumption per number of exposed surface metallic copper sites in the initial reaction stage of 15 min (FFA conversions were controlled to less than 30 % by reducing the amount of catalyst to 0.01 g under the same reaction conditions) (Table S1). As shown in Fig.7A, the TOF value increases gradually with the increase in the metallic copper surface area. The significant difference in the TOF value among Cu/ZrO₂ catalysts strongly demonstrate that metallic copper species are not the sole catalytically active sites in the FFA hydrogenation. For the FFA hydrogenation process, the carbonyl oxygen of FFA with lone pair electrons can adsorb on electrophilic Cu⁺ sites on the surface of Cu/ZrO₂ catalysts, thereby promoting the activation of the C=O bond in FFA [26,29,36]. Correspondingly, besides surface metallic copper species, surface Cu⁺ species can greatly improve the activity of the present Cu/ZrO₂ catalysts. Further, the variations in the CPO selectivity at different reaction time as a function of surface Cu⁺/(Cu⁰+Cu⁺) ratio on different Cu/ZrO₂ catalysts are plotted (Fig.7B). Notably, despite different reaction times, the CPO selectivity presents a good linear trend with surface Cu⁺/(Cu⁰+Cu⁺) ratio, indicating that surface Cu⁺ species may facilitate the FAL rearrangement. Moreover, the initial rate of CPO formation at low conversion levels was determined by using a

reduced amount of catalyst (Table S1). As shown in Fig.7C, the higher surface $\text{Cu}^+ / (\text{Cu}^0 + \text{Cu}^+)$ ratio, the faster the initial rate of CPO generation. Obviously, the highest initial rate of CPO formation is obtained over the Cu/ZrO₂-500. It indicates that the formation of CPO is closely related to Cu⁺ species. Under the same reaction conditions, however, no CPO can be generated over the Cu/ZrO₂-600 after a reaction time of 15 min, due to its poor hydrogenation activity. The above results confirm that surface $\text{Cu}^+ / (\text{Cu}^0 + \text{Cu}^+)$ ratio on Cu/ZrO₂ catalysts can play a key role in promoting the formation of CPO product.

Furthermore, the effect of the reaction temperature on the FFA conversion and product selectivities over the Cu/ZrO₂-500 was explored. As shown in Fig.8A, one can see that in addition to target CPO product, a large amount of FAL intermediate is produced at a low reaction temperature of 130 °C. With the increasing reaction temperature to 150 °C, Cu/ZrO₂-500 delivers a high CPO yield of 91.3 %. According to the literature [53], the ionization constant of water (pKa) at 150°C is about 11.6, indicating that the high temperature is beneficial to the dissociation of water as an endothermic reaction. Moreover, it was reported that the high reaction temperatures could contribute to the rearrangement of FFA to 4-hydroxycyclopentenone(4-HCP) [54], another intermediate, during the FFA hydrogenation into CPO. It is expected that an additional effect of the acidity of water should be substantial at the high reaction temperature of 150 °C, thus promoting the formation of CPO to a large extent in our case. This is consistent with our experimental results that high reaction temperature is conducive to accelerate the FAL rearrangement and promote the CPO formation. Further increase in the reaction temperature, however, leads to a gradual decline in the CPO selectivity, due to the easier deep hydrogenation of CPO. Therefore, it is concluded that the appropriate reaction temperature of 150 °C is beneficial to the FAL rearrangement and the generation of CPO product. Moreover, we further investigated the effect of hydrogen pressure on the FFA conversion and product selectivities (Fig.8B). Noticeably, with the increasing hydrogen pressure from 0.5 to 1.5 MPa, the CPO selectivity increases gradually from 54.5 % to 91.3 %, whereas the selectivities of FAL and 2-CPEO intermediates present an opposite trend, despite the formation of a small amount of CPL.

As the hydrogen pressure is further increased to 2.0 MPa, the CPO selectivity begins to decline due to the generation of more CPL. As a result, the high hydrogen pressure can facilitate the hydrogenation of both the C=O and C=C bonds in reactants and intermediates.

The stability of Cu/ZrO₂-500 also was examined (Fig.S5), the catalyst can maintain a high activity in the FFA hydrogenation after five successive cycles, along with high conversions of above 99 %, and the CPO selectivity is decreased only by about 2.5%. The XRD patterns, Cu 2p XPS and Cu LMM XAES (Fig.S6) of used Cu/ZrO₂-500 catalyst reveal that there is almost no change in the XRD patterns of Cu/ZrO₂-500 after five successive runs, and the relative proportion of surface Cu⁺ species in total copper species also almost keeps unchanged. In addition, elemental analysis by ICP-AES shows that the decrease in the Cu content in the catalyst is only 0.4 wt % after five runs (Table S2), indicating that there is a slight loss of the active composition due to a slight solubility of active Cu species in the reaction medium, thereby causing a slight decrease in the activity. And, TEM images of the used catalyst show that the size of Cu particles does not change significantly after five runs (Fig.S6). The above results demonstrate the good stability of Cu/ZrO₂-500 catalyst.

3.4 Mechanistic study on the FFA hydrogenation

To study the reaction mechanism of the FFA hydrogenation over Cu/ZrO₂ catalysts, a series of controlled reactions were further tested (Table 3). In the FFA hydrogenation, the FAL rearrangement is a key step in generating target CPO product. Therefore, the hydrogenation of FAL as substrate also was examined over different catalysts (Table 3, entries 1-4). In the absence of any catalysts, a quite low FAL conversion of 2.5 % is obtained (Table 3, entry 1). One can see that pure ZrO₂-500 and Cu/ZrO₂-R afford the FAL conversions of 8.1 % and 65.7 %, respectively, along with the CPO selectivities of 36.9 % and 67.5 % (Table 3, entries 2 and 3). Cu/ZrO₂-500 (Table 3, entry 4) yields a greatly increased FAL conversion of 97.8 %. To determine the effect of surface acidic sites on the above reaction, surface Brønsted/Lewis acidic sites on the Cu/ZrO₂-500 catalyst was blocked by pyridine. First, the catalyst was soaked in pyridine for 15 min.

Subsequently, the catalyst was purged with nitrogen gas and then dried at room temperature for 12 h under vacuum. Finally, the reaction was carried out over the poisoned catalyst. Noteworthy, after surface acidic sites on the Cu/ZrO₂-500 was blocked by pyridine, the FFA conversion slightly decreases but the CPO selectivity drops rapidly from 62.7 % to 40.3 % (Table 3, entries 5 and 6). It demonstrates that surface acidity of catalysts is beneficial to the formation of CPO. The above results further illustrate that both Cu⁺ species and surface acidity can promote the FAL rearrangement and thus the production of CPO.

For comparison, other different metal oxides (*i.e.* ZrO₂, Al₂O₃, MgO, and ZnO) supported copper catalysts were synthesized by the conventional impregnation (Fig.S7, S8 and S9). As shown in Fig S8, surface acidity of ZrO₂ is significantly higher than those of amphoteric Al₂O₃ and ZnO [43]. As expected, basic MgO presents a rather weak acidity. As shown in Table 4, the CPO selectivities over Cu/ZrO₂-im and Cu/Al₂O₃-im are much lower than that over the present Cu/ZrO₂-500, which should be associated with less surface Cu⁺ species on Cu/ZrO₂-im and Cu/Al₂O₃-im. Meanwhile, compared with Cu/ZrO₂-im and Cu/Al₂O₃-im, Cu/ZnO-im affords a much lower selectivity to CPO, due to its weaker surface acidity. Especially, almost no CPO can be produced over the Cu/MgO-im, which is correlated with the absence of surface Cu⁺ species and acidic sites. Although Cu/ZnO-im possesses the similar amount of surface Cu⁺ species to that on the Cu/Al₂O₃-im, Cu/ZnO-im delivers a much lower CPO selectivity. The above results further demonstrate that both favorable surface acidity and abundant Cu⁺ species on catalysts can significantly promote the FAL rearrangement to form CPO in the FFA hydrogenation.

Based on the above characteristic and experimental results, a possible catalytic mechanism for the FFA hydrogenation to CPO over Cu/ZrO₂ catalysts is proposed (Fig.9). Firstly, surface highly dispersed Cu⁰ species as active centers can dissociate molecular hydrogen and thus provide available active hydrogen species for reducing the C=O bond in FFA to generate FAL. Meanwhile, Cu⁺ species as electrophilic centers can polarize the C=O bond of FFA through the isolated electron pair of carbonyl oxygen. In a way, surface Lewis acidic sites can serve as electron acceptors to accept the electron on the carbonyl group, which facilitates the attack of

active hydrogen species to the C=O bond and not to the C=C double bond in furan ring [55]. Subsequently, the FAL rearrangement can proceed through the self-dissociation of water to generate 2-CPEO intermediate. During FAL rearrangement, weak Lewis acidic sites are beneficial to the formation and stability of formed carbocation species [56], while Cu^+ species are beneficial to the stability of formed oxycation species [26,54]. Finally, CPO is produced by the hydrogenation of 2-CPEO. As a result, unique surface synergistic effect between Cu^+ species and acidic sites on Cu/ZrO_2 catalysts is the key to achieve the high CPO selectivity in the present catalytic system.

4. Conclusions

In summary, series of Cu/ZrO_2 catalysts synthesized by our developed one-pot reduction-oxidation route were employed in the conversion of FFA to produce CPO in water. By adjusting the calcination temperature of catalyst precursors, surface structures and catalytic performances of Cu/ZrO_2 catalysts could be delicately regulated. It was found that the Cu/ZrO_2 catalyst obtained at the calcination temperature of 500 °C exhibited a superior catalytic performance with a high CPO yield of 91.3 % to other supported Cu/ZrO_2 ones under mild reaction conditions (*i.e.* a low hydrogen pressure of 1.5 MPa and 150 °C). Combining a series of structural characterizations with catalytic experimental results, we revealed that an appropriate calcination temperature of 500 °C could significantly improve the interactions between Cu species and the ZrO_2 support, thus forming $\text{Cu}^+\text{-O-Zr}$ -like structure at the metal-support interface. Surface synergy between acidic sites and Cu^+ species on Cu/ZrO_2 catalysts greatly promoted the rearrangement of FAL intermediate and thus the formation of high-yield target CPO product in the present catalytic system. The present findings provide a high performing supported copper catalyst for the conversion of FAL into CPO in water, while as-constructed surface synergistic effect between Cu^+ species and acidic sites open a new idea for the design of other metal catalysts for the biomass transformations through catalytic hydrogenation/hydrogenolysis processes. Such

readily available, highly efficient and stable Cu-based heterogeneous catalyst possesses promising potential for the industrial application.

Acknowledgments

This study was funded through National Natural Science Foundation of China (21776017;21521005) and Fundamental Research Funds for the Central Universities (buctrc201528).

Appendix A. Supplementary data

Supplementary data associated with this article can be found, in the online version, at <http://dx.doi.org/10.1016/j.apcata.xxxx>.

References

- [1] L. P. Koh, J. Ghazoul, *Biol. Conserv.* 141 (2008) 2450-2460.
- [2] E. M. Jamal, *Renew. Y. Sust. Energ. Rev.* 15 (2011) 4732-4745.
- [3] W. J. Liu, W. W. Li, H. Jiang, H. Q. Yu, *Chem. Rev.* 117 (2017) 6367-6398.
- [4] E. I. Gurbuz, J. M. Gallo, D. M. Alonso, S. G. Wettstein, W. Y. Lim, J. A. Dumesic, *Angew. Chem.* 52 (2013) 1270-1274.
- [5] V. Choudhary, S. I. Sandler, D. G. Vlachos, *ACS Catal.* 2 (2012) 2022-2028.
- [6] N. K. Gupta, A. Fukuoka, K. Nakajima, *ACS Catal.* 7 (2017) 2430-2436.
- [7] K. Yan, G. Wu, T. Lafleur, C. Jarvis, *Renew. Sust. Energ. Rev.* 38 (2014) 663-676.
- [8] R. Mariscal, P. Maireles-Torres, M. Ojeda, I. Sádaba, M. L. Granados, *Energ. Environ. Sci.* 9 (2016) 1144-1189.
- [9] X. Li, P. Jia, T. Wang, *ACS Catal.* 6 (2016) 7621-7640.
- [10] S. A. Khromova, M. V. Bykova, O. A. Bulavchenko, Y. D. Ermakov, A. A. Saraev, V. V. Kaichev, R. H. Venderbosch, V. A. Yakovlev, *Top. Catal.* 59 (2016) 1413-1423.

- [11] N. S. Biradar, A. M. Hengne, S. N. Birajdar, P. S. Niphadkar, P. N. Joshi, C. V. Rode, *ACS Sustainable. Chem. Eng.* 2 (2014) 272-281.
- [12] W. S. Lee, Z. Wang, W. Zheng, D. G. Vlachos, A. Bhan, *Catal. Sci. Technol.* 4 (2014) 2340-2352.
- [13] M. J. Gilkey, P. Panagiotopoulou, A. V. Mironenko, G. R. Jenness, D. G. Vlachos, B. Xu, *ACS Catal.* 5 (2015) 3988-3994.
- [14] S. Sitthisa, D. E. Resasco, *Catal. Lett.* 141 (2011) 84-791.
- [15] S. Zhu, Y. Xue, J. Guo, Y. Cen, J. Wang, W. Fan, *ACS Catal.* 6 (2016) 2035-2042.
- [16] L. Bui, H. Luo, W. R. Gunther, Y. R. Leshkov, *Angew. Chem.* 52 (2013) 8022-8025.
- [17] T. Mizugaki, T. Yamakawa, Y. Nagatsu, Z. Maeno, T. Mitsudome, K. Jitsukawa, K. Kaneda, *ACS Sustainable. Chem. Eng.* 2 (2014) 2243-2247.
- [18] J. Scognamiglio, L. Jones, C. S. Letizia, A. M. Api, *Food chem. Toxicol.* 50 (2012) 608-612.
- [19] W. Wang, X. Ji, H. Ge, Z. Li, G. Tian, X. Shao, Q. Zhang, *RSC Adv.* 7 (2017) 16901-16907.
- [20] J. Yang, N. Li, G. Li, W. Wang, A. Wang, X. Wang, Y. Cong, T. Zhang, *Chem. Commun.* 50 (2014) 2572-2574.
- [21] M. Renz, *Eur. J. Org. Chem.* 2005 (2005) 979-988.
- [22] K.A. Dubkov, G.I. Panov, E.V. Starokon, V. N. Parmon, *Catal. Lett.* 77 (2002) 197-205.
- [23] J. Marquié, A. Laporterie, J. Dubac, N. Roques, *Synlett* 2001 (2001) 0493-0496.
- [24] M. Hronec, K. Fulajtarová, *Catal. Commun.* 24 (2012) 100-104.
- [25] M. Hronec, K. Fulajtárova, M. Mičušík, *Appl. Catal. A: Gen.* 468 (2013) 426-431.
- [26] M. Hronec, K. Fulajtárova, I. Vávra, T. Soták, E. Dobročka, M. Mičušík, *Appl. Catal. B: Environ.* 181 (2016) 210-219.
- [27] G. S. Zhang, M. M. Zhu, Q. Zhang, Y. M. Liu, H. Y. He, Y. Cao, *Green Chem.* 18 (2016) 2155-2164.
- [28] Y. Liu, Z. Chen, X. Wang, Y. Liang, X. Yang, Z. Wang, *ACS Sustainable. Chem. Eng.* 5 (2016) 744-751.

- [29] X. L. Li, J. Deng, J. Shi, T. Pan, C. G. Yu, H. J. Xu, Y. Fu, *Green Chem.* 17 (2015) 1038-1046.
- [30] M. Zhou, J. Li, K. Wang, H. Xia, J. Xu, J. Jiang, *Fuel* 202 (2017) 1-11.
- [31] J. Guo, G. Xu, Z. Han, Y. Zhang, Y. Fu, Q. Guo, *ACS Sustainable. Chem. Eng.* 2 (2014) 2259-2266.
- [32] Y. Yang, Z. Du, Y. Huang, F. Lu, F. Wang, J. Gao, J. Xu, *Green Chem.* 15 (2013) 1932-1940.
- [33] Y. Wang, S. Sang, W. Zhu, L. Gao, G. Xiao, *Chem. Eng. J.* 299 (2016) 104-111.
- [34] H. Zhu, M. Zhou, Z. Zeng, G. Xiao, R. Xiao, *Korean J. Chem. Eng.* 31 (2014) 593-597.
- [35] R. S. Rao, R. T. K. Baker, M. A. Vannice, *Catal. Lett.* 60 (1999) 51-57.
- [36] Y. J. Xu, J. Sh, W. P. Wu, R. Zhu, X. L. Li, J. Deng, Y. Fu, *Appl. Catal. A: Gen.* 543 (2017) 266-273.
- [37] R. T. Figueiredo, A. Martínez-Arias, M. L. Granados, J. L. G. Fierro, *J. Catal.* 178 (1998) 146-152
- [38] L. Chen, P. Guo, M. Qiao, S. Yan, H. Li, W. Shen, H. Xu, K. Fan, *J. Catal.* 257 (2008) 172-180.
- [39] S. Wang, H. Liu, *Catal. Lett.* 117 (2007) 62-67.
- [40] A. Y. Yin, X. Y. Guo, W. L. Dai, K. N. Fan, *J. Catal.* 277 (2011) 54-63
- [41] S. S. Liu, G. Fan, L. Yang, F. Li, *Appl. Catal. A: Gen.* 543 (2017) 180-188.
- [42] W. Li, Y. Li, G. Fan, L. Yang, F. Li, *ACS Sustainable. Chem. Eng.* 5 (2017) 2282-2291.
- [43] Y. Wang, W. Zhu, S. Sang, L. Gao, G. Xiao, *Asia-Pac. J. Chem. Eng.* 12 (2017) 422-431.
- [44] X. C. Zhou, W. L. Xu, G. K. Liu, D. Panda, P. Chen, *J. Am. Chem. Soc.* 132 (2010), 138-146
- [45] Y. Y. Cui, B. Wang, C. Wen, X. Chen, W.-L. Dai, *ChemCatChem.* 8 (2016), 527-531
- [46] J. Zhou, Z. Hua, J. Shi, Q. He, L. Guo, M. Ruan, *Chem. Eur. J.* 15 (2009) 12949-12954.
- [47] S. Zhao, H. Yue, Y. Zhao, B. Wang, Y. Geng, J. Lv, S. Wang, J. X. Gong, *J. Catal.* 297 (2013) 142-150.

- [48] J. Gong, H. Yue, Y. Zhao, S. Zhao, L. Zhao, J. Lv, S. Wang, X. Ma, *J. Am. Chem. Soc.* 134 (2012) 13922-13925.
- [49] A. Yin, X. Guo, W. L. Dai, K. Fan, *J. Phys. Chem. C.* 113 (2009) 11003-11013.
- [50] G. S. Rao, N. P. Rajan, M. H. Sekha, S. Ammaji, K. V. R. Chary, *J. Molec. Catal. A: Chem.* 395 (2014) 486-493.
- [51] J. Zuo, Z. Chen, F. Wang, Y. Yu, L. Wang, X. Li, *Ind. Eng. Chem. Res.* 53 (2014) 2647-2655.
- [52] H. Xu, Q. Zhang, C. Qiu, T. Lin, M. Gong, Y. Chen, *Chem. Eng. Sci.* 76 (2012) 120-128.
- [53] A. V. Bandura, S. N. Lvov, *J. Phys. Chem. Ref. Data*, Vol. 35, No.1 (2006).
- [54] M. Hronec, K. Fulajtárová, T. Soták, *J. Ind. Eng. Chem.* 20 (2014) 650-655.
- [55] S. Sitthisa, T. Sooknoi, Y. Ma, P. B. Balbuena, D. E. Resasco, *J. Catal.* 277 (2011) 1-13.
- [56] M. Hronec, K. Fulajtarová, T. Liptaj, *Appl. Catal. A: Gen.* 437-438 (2012) 104-111.

Table

Table 1 The compositional and structural properties of samples.

Samples	Content (wt.%) ^a	S _{BET} ^b	D ₁₁₁ ^c	S _{Cu} ^d	S _{Cu⁺} ^e	Cu ⁺ / (Cu ⁰ +Cu ⁺)	Specific acidity ^f
---------	-----------------------------	-------------------------------	-------------------------------	------------------------------	--	---	-------------------------------

	Cu	Zr	(m ² /g)	(nm)	(m ² /g)	(m ² /g)	Ratio ^e	(mmol/g) ^g
Cu/ZrO ₂ -R	25.9	23.5	115	20.2	23.6	13.9	0.37	0.46 (0.30) ^g
Cu/ZrO ₂ -400	26.1	24.8	108	24.0	21.6	19.9	0.48	0.32 (0.21)
Cu/ZrO ₂ -500	26.0	24.5	93	25.2	18.5	18.5	0.50	0.30 (0.22)
Cu/ZrO ₂ -600	26.7	25.1	58	30.9	6.0	4.5	0.43	0.14 (0.13)

^a Determined by ICP-AES; ^b Specific surface area calculated by the BET method; ^c Average crystallite size of metallic Cu particles estimated from XRD patterns; ^d Metallic copper surface area determined by N₂O titration; ^e Determined by Cu LMM XAES analysis; ^f Density of total acidic sites determined by NH₃-TPD; ^g Density of weak acidic sites determined by NH₃-TPD.

Table 2 Catalytic results of Cu/ZrO₂ catalysts for the FFA hydrogenation. ^a

Catalysts	Time (h)	Conv. (%)	Selectivity (%)				
			CPO	CPL	FAL	2-CPEO	Others ^b
Cu/ZrO ₂ -R	0.5	100	16.0	0	82.8	0.6	0.6
	4.0	100	45.7	15.9	37.7	0	0.7
Cu/ZrO ₂ -400	0.5	100	19.2	0	72.4	6.1	2.3
	4.0	100	89.9	4.2	1.9	0.9	3.1
Cu/ZrO ₂ -500	0.5	77.1	18.2	0	73.3	6.8	1.7
	4.0	100	91.3	3.8	1.4	1.4	2.1
Cu/ZrO ₂ -600	0.5	75.5	8.9	0	87.0	3.0	1.1
	4.0	100	71.2	3.5	23.1	0.8	1.4

^a Reaction conditions: catalyst, 0.05 g; FFA, 5 mmol; H₂O, 15 ml; reaction temperature, 150 °C; hydrogen pressure, 1.5 MPa. ^b Oligomers by-product.

Table 3 Catalytic results of Cu/ZrO₂ catalysts for the FAL or FFA hydrogenation. ^a

Entry	Catalysts	Substrates	Conv.	Selectivity (%)
-------	-----------	------------	-------	-----------------

			(%)	CPO	CPL	FAL	2-CPEO	Others
1	blank	FAL	2.5	7.1	0	--	30.3	62.6
2	ZrO ₂ -500	FAL	8.1	36.9	0	--	2.1	61.0
3	Cu/ZrO ₂ -R	FAL	65.7	67.5	24.9	-	0	7.6
4	Cu/ZrO ₂ -500	FAL	97.8	77.6	18.5	-	0.5	3.4
5 ^b	Cu/ZrO ₂ -500	FFA	98.2	62.7	0.7	25.6	9.2	1.8
6 ^c	Cu/ZrO ₂ -500	FFA	95.9	40.3	0.2	54.9	2.5	2.1

^a Reaction conditions: catalyst, 0.05 g; FAL or FFA, 5 mmol; H₂O, 15 ml; reaction temperature, 150 °C; hydrogen pressure, 1.5 MPa; reaction time, 4 h. ^b Reaction time, 1.5 h.

^c catalyst was poisoned by pyridine before reaction; reaction time, 1.5h.

Table 4 Catalytic results of metal oxides supported copper catalysts for FFA hydrogenation ^a

Entry	Catalyst	D ₁₁₁ ^b (nm)	S _{Cu} ^c (m ² /g)	Cu ⁺ / (Cu ⁰ +Cu ⁺) Ratio ^d	Conv. (%)	Selectivity (%)			
						CPO	CPL	FAL	Others
1	Cu/ZrO ₂ -500	25.2	18.5	0.50	100	91.3	3.8	1.4	3.5
2	Cu/ZrO ₂ -im	28.6	12.6	0.33	90.8	67.0	1.0	18.9	13.1
3	Cu/Al ₂ O ₃ -im	27.2	11.3	0.29	99.7	42.9	1.5	50.5	5.1
4	Cu/MgO-im	25.7	14.7	0	100	0.6	0.3	98.5	0.6
5	Cu/ZnO-im	34.8	9.2	0.30	63.2	3.9	0	86.3	9.8

^a Reaction conditions: catalyst, 0.05 g; FFA, 5 mmol; H₂O, 15 ml; reaction temperature, 150 °C; hydrogen pressure, 1.5 MPa; reaction time, 4h. ^b Average crystallite size of metallic Cu particles estimated from XRD patterns; ^c Metallic copper surface area determined by N₂O titration; ^d Determined by XAES analysis.

Figure captions

Fig.1 XRD patterns of CuO/ZrO₂ precursors (A) and Cu/ZrO₂ samples (B) obtained at different calcination temperatures: (a) room temperature, (b) 400 °C, (c) 500 °C and (d) 600 °C.

Fig.2 TEM images of Cu/ZrO₂-R (A), Cu/ZrO₂-400 (B), Cu/ZrO₂-500 (C) and Cu/ZrO₂-600 (D) samples.

Fig.3 H₂-TPR profiles of CuO/ZrO₂-R (a), CuO/ZrO₂-400 (b), CuO/ZrO₂-500 (c) and CuO/ZrO₂-600 (d).

Fig.4 Cu 2p XPS (A) and Cu LMM XAES (B) of Cu/ZrO₂-R (a), Cu/ZrO₂-400 (b), Cu/ZrO₂-500 (c) and Cu/ZrO₂-600 (d) samples.

Fig.5 *in situ* IR spectra of adsorbed pyridine (A) and NH₃-TPD curves (B) over pristine ZrO₂-500 (a) and Cu/ZrO₂-R (b), Cu/ZrO₂-400 (c), Cu/ZrO₂-500 (d) and Cu/ZrO₂-600 (e) samples.

Fig.6 Change in the conversion and product selectivities in the FFA hydrogenation with the reaction time over Cu/ZrO₂-R (A), Cu/ZrO₂-400 (B), Cu/ZrO₂-500 (C) and Cu/ZrO₂-600 (D). Reaction conditions: reaction temperature, 150 °C; hydrogen pressure, 1.5 MPa.

Fig.7 The variation in the TOF value of FFA conversion as a function of metallic copper surface area for Cu/ZrO₂ catalysts (A), the variations in the CPO selectivity as a function of surface Cu⁺/(Cu⁰+Cu⁺) ratio on Cu/ZrO₂ catalysts at different reaction times (B), and the variations in the initial rate of CPO formation as a function of surface Cu⁺/(Cu⁰+Cu⁺) ratio in the reaction stage of 15 min (C). Reaction conditions: reaction temperature, 150 °C; hydrogen pressure, 1.5 MPa.

Fig.8 Change of FFA conversion and product selectivities over the Cu/ZrO₂-500 in the FFA hydrogenation at different reaction temperatures (A) and different hydrogen pressures (B).

Fig.9 Proposed reaction mechanism for the catalytic FFA hydrogenation to CPO over Cu/ZrO₂ catalysts.

